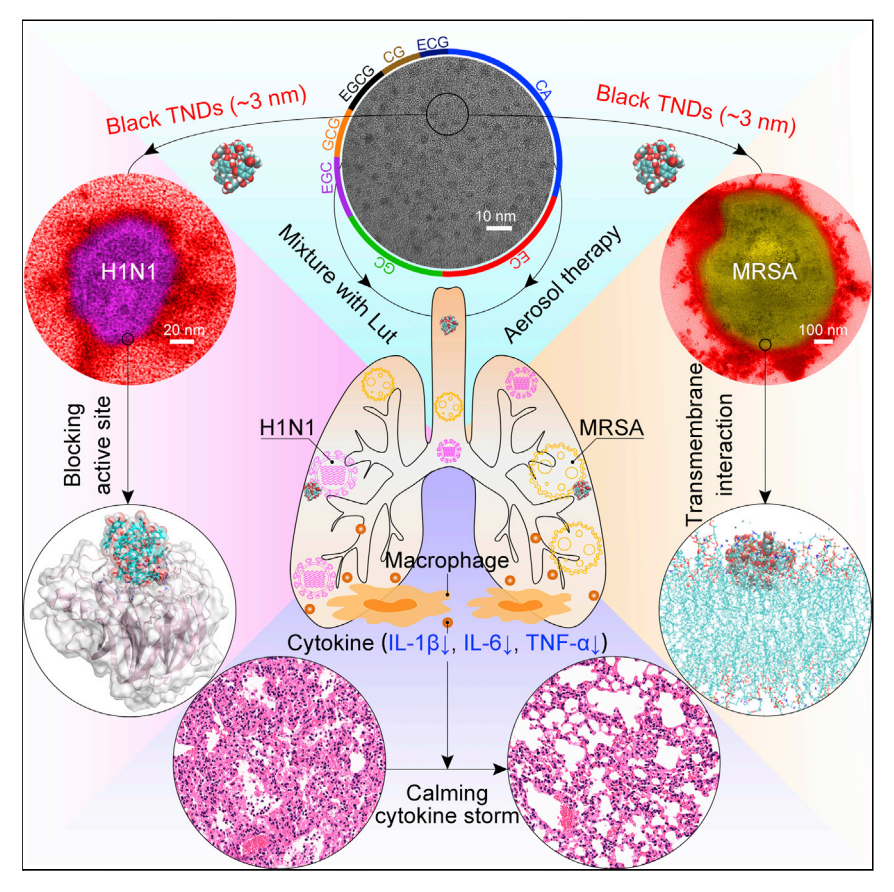
Matter



Article

Material-herbology: An effective and safe strategy to eradicate lethal viral-bacterial pneumonia



We propose the concept of material-herbology strategy by using materialogy methods to enhance the therapeutic effect of herbal medicines. Specifically, tea nanodots with an average size of ~3 nm containing eight kinds of tea catechins were able to kill MRSA (by physical transmembrane interaction and inhibition of amino acid metabolism), eradicate H1N1 (by blocking neuraminidase active site), and calm cytokine storms (by antioxidant-related anti-inflammatory effect), resulting in a 100% recovery rate from lethal MRSA-H1N1 pneumonia when combined with luteolin.

Jun Li, Ziao Zhou, Xiangmei Liu, ..., Yanqin Liang, Xianbao Wang, Shuilin Wu

liuxiangmei1978@163.com (X.L.) shuilin.wu@gmail.com, shuilinwu@tju.edu.cn (S.W.)

Highlights

Material-herbology is the interdisciplinary concept of materials science and herbology

Antibacterial mechanism is transmembrane interactions and targets of amino acids

Antiviral mechanism against H1N1 is inhibition of the active site of neuraminidase

The strategy shows excellent therapeutic effects for lethal H1N1-MRSA pneumonia



Li et al., Matter 4, 3030–3048 September 1, 2021 © 2021 Elsevier Inc. https://doi.org/10.1016/j.matt.2021.07.001







Article

Material-herbology: An effective and safe strategy to eradicate lethal viral-bacterial pneumonia

Jun Li,¹ Ziao Zhou,² Xiangmei Liu,^{2,*} Yufeng Zheng,³ Changyi Li,⁴ Zhenduo Cui,¹ Kelvin Wai Kwok Yeung,⁵ Hongbo Zhou,⁶ Jiahui Zou,⁶ Zhaoyang Li,¹ Shengli Zhu,¹ Yanqin Liang,¹ Xianbao Wang,² and Shuilin Wu^{1,7,*}

SUMMARY

Clinically, lethal viral-bacterial pneumonia is a severe threat to human health worldwide. Here, for the first time, we propose a "material-herbology" strategy, in which herbal medicines are utilized as materials or refreshed by using materialogy methods to enhance their therapeutic effect. Specifically, in this work, natural tea nanodots (TNDs, with an average size of ~3 nm) are made from several kinds of catechins extracted from Chinese black tea (Black TNDs). The antibacterial mechanism (transmembrane interactions and specific targets of amino acids) against methicillin-resistant Staphylococcus aureus (MRSA) and antiviral mechanism (inhibition of the active site of neuraminidase) against H1N1 are explored. The Black TNDs had excellent biosafety in piglets, and in combination with luteolin the optimized synergistic aerosol therapy exhibited greater advantage against lethal H1N1-MRSA pneumonia than the reported clinical therapy, owing to the rapid clearance of H1N1 and MRSA as well as the antioxidant-related anti-inflammatory effect.

INTRODUCTION

Annually, the seasonal influenza virus causes 290,000–650,000 deaths worldwide, ¹ most of which are cases that gradually evolve from initial viral respiratory tract infection into viral-bacterial pneumonia.^{2,3} Clinically, viral-bacterial pneumonia contributes to very high mortality because of complex interactions between pathogens and the host.^{2,3} During the global pandemic of the novel coronavirus pneumonia (COVID-19), almost all patients with serious COVID-19 were treated with antibiotics due to secondary bacterial infection, and many patients have died of bacterial superinfection, including multidrug-resistant (MDR) bacterial infections, rather than the virus itself.^{4,5} Similarly, almost all deaths in the 1918 influenza pandemic (about 50 million worldwide) were caused by bacterial coinfection,^{4,6} and based on published autopsy series, 55% of fatal cases had bacterial coinfections in the 2009 influenza (H1N1) pandemic, which led to approximately 280,000 deaths worldwide.^{4,6} Moreover, viral-bacterial pneumonia in these global pandemics is usually accompanied by lethal hyperinflammation and cytokine storm syndrome.^{2,3}

The high mortality of viral-bacterial pneumonia results from three major factors: (1) influenza viruses can inhibit an immune response to a secondary bacterial infection, consequently inducing increases in bacterial load and the death rate;² (2) almost all currently used antibiotics with safe dosage are ineffective against these MDR bacteria;⁷ and (3) prolonged hyperinflammation and overactivated cytokines disrupt the

Progress and potential

Clinically, viral-bacterial pneumonia contributes to very high mortality because of complex interactions between pathogens and the host. Here, the material-herbology strategy, using materialogy methods to enhance the therapeutic effect of herbal medicines, serves as a safe and effective therapeutic strategy to eradicate both viral and bacterial pathogens without inflammation-induced tissue damage when treating lethal viralbacterial pneumonia. The antibacterial mechanism (transmembrane interactions and specific targets of amino acids) and antiviral mechanism against H1N1 (inhibition of the active site of neuraminidase) are explored. To sum up, the materialherbology strategy, by combining materialogy with herbology of Chinese medicine against various bacterial and viral diseases in clinical research, may play a positive role in reducing infectious mortality in the near future, and not only for viral-bacterial pneumonia.







host immune system and homeostasis.^{2,3} Therefore, a safe and effective therapeutic strategy to eradicate both viral and bacterial pathogens without inflammation-induced tissue damage and drug resistance is urgently needed for treating lethal viral-bacterial pneumonia in a short period of time.

Currently, the pharmaceutical offerings of new antibiotics or antiviral drugs for clinical practice are typically expensive and take several years to develop, while it only takes bacteria or viruses a short time to evolve resistance against newly developed drugs. 8–11 Screening new antiviral and antibacterial agents originating from biosafe natural materials is a critical way to broaden such possibilities; in fact, a majority of the antibacterial or antiviral drugs developed from natural products have been listed as essential medicines. 11,12 Chinese herbal medicines have been employed to cure various kinds of diseases in China since ancient times, including Huperzine A for treatment of Alzheimer's disease and antimalarial artemisinin. Moreover, COVID-19 can be treated by the Lianhua Qingwen capsule. Hence, it is possible to screen appropriate Chinese herbal medicines to determine their ability to overcome these challenges. 15

As one kind of Chinese herbal medicine, tea has been consumed for more than 4,500 years in China. ^{16,17} At present, the global population consumes over 2 billion cups of tea daily. ^{17,18} The annual tea yields are over 5 million tons throughout the world, and this industry is on the rise. ^{17,19} Tea and related products have been reported to possess multiple health benefits, including mental health improvement, antioxidative action, cancer prevention, antiviral effects, and antibacterial activity. ^{19–22} Besides tea, many other Chinese herbal medicines have antiviral and antibacterial effects, such as berberine (Ber), quercetin (Que), and luteolin (Lut). However, the limited success in clinical practice of Chinese herbal medicine and its extracts has highlighted the inherent difficulties in studying its cheminformatics and bioinformatics. Specifically, Chinese herbal medicine and its extracts composed of complex chemical components, including tea catechins, have unclear pharmacological data and unknown drug targets. ²² In addition, their therapeutic efficiency and biosafety remain in need of further improvement.

Here, for the first time, we propose a strategy of material-herbology, in which herbal medicines are utilized as biological functional materials or refreshed by using materialogy methods to enhance their therapeutic effect. In this work, based on this concept, two kinds of Chinese herbal medicines, natural tea extracts and Lut, were utilized to treat lethal H1N1 methicillin-resistant Staphylococcus aureus (H1N1-MRSA) pneumonia by aerosol therapy. The natural tea extracts existed in the form of tea nanodots (TNDs) of ~3 nm, which were mainly composed of eight kinds of catechins extracted from black Chinese tea by a nanotechnology-inspired strategy (Black TNDs). As shown in Figure 1, the physical and biological antibacterial mechanisms of Black TNDs against MRSA were transmembrane interaction and specific targets of amino acids, respectively, and the platform exhibited a low probability of developing bacterial resistance over 100 serial passages. Black TNDs also showed effective antiviral activity against H1N1 by inhibiting the active sites of neuraminidase. Moreover, Black TNDs had excellent biosafety in piglets. Inspired by Chinese medicinal formula compatibility and combining Black TNDs with Lut, the optimized synergistic aerosol therapy exhibited a greater advantage against lethal H1N1-MRSA pneumonia than clinical therapy, owing to rapid H1N1 and MRSA clearance and antioxidant-related anti-inflammatory effects. Therefore, material-herbology not only exhibits great potential as a valuable alternative to current therapies in clinical practice against lethal H1N1-MRSA pneumonia but could also bring fresh

¹School of Materials Science & Engineering, the Key Laboratory of Advanced Ceramics and Machining Technology by the Ministry of Education of China, Tianjin University, Tianjin 300072, China

²Ministry-of-Education Key Laboratory for the Green Preparation and Application of Functional Materials, Hubei Key Laboratory of Polymer Materials, School of Materials Science & Engineering, Hubei University, Wuhan 430062, China

³State Key Laboratory for Turbulence and Complex System and Department of Materials Science and Engineering, College of Engineering, Peking University, Beijing 100871, China

⁴Stomatological Hospital, Tianjin Medical University, No. 12, Qixiangtai Road, Heping District, Tianjin 300070, China

⁵Department of Orthopaedics & Traumatology, Li Ka Shing Faculty of Medicine, The University of Hong Kong, Pokfulam, Hong Kong 999077, China

⁶State Key Laboratory of Agricultural Microbiology, College of Veterinary Medicine, Huazhong Agricultural University, Wuhan 430070, China

⁷Lead contact

*Correspondence:

liuxiangmei1978@163.com (X.L.), shuilin.wu@gmail.com, shuilinwu@tju.edu.cn (S.W.)

https://doi.org/10.1016/j.matt.2021.07.001





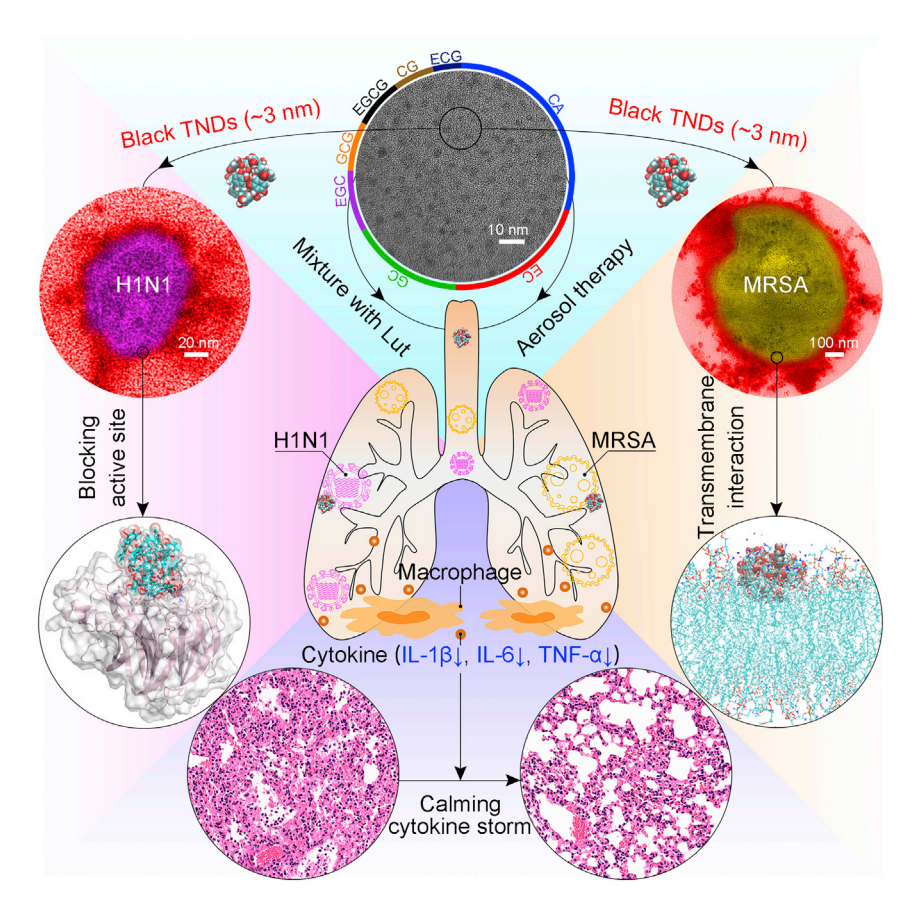


Figure 1. Schematic illustration of therapy for lethal H1N1-MRSA pneumonia through strategy of Chinese material-herbology

Black TNDs with an average size of ~3 nm containing eight kinds of tea catechins were able to kill MRSA (by physical transmembrane interaction and inhibition of amino acid metabolism), eradicate H1N1 (by blocking NA active site), and calm cytokine storm (by antioxidant-related anti-inflammatory effect), resulting in a 100% recovery rate from lethal MRSA-H1N1 pneumonia when Black TNDs were combined with Lut.

insights into disciplines such as materials science, physics, and pharmaceutical science to help tackle infectious diseases through the use of herbal medicines.

RESULTS AND DISCUSSION

Screening and characterization of six kinds of TNDs

To prepare and screen TNDs with the optimized therapeutic effect, we extracted the six kinds of TNDs (Black TNDs, Dark TNDs, Green TNDs, Oolong TNDs, White TNDs, and Yellow TNDs) from six corresponding kinds of Chinese tea (black tea, dark tea, green tea, oolong tea, white tea, and yellow tea), as shown in Figures S1–S10. This nanotechnology-inspired strategy was achieved via a hydrothermal method by modulating the reaction temperature, pressure, and time. Overall, they had similar morphology and components. As shown in Table S1, the minimum inhibitory concentrations (MICs) of the six kinds of Chinese tea and English black tea were measured against *S. aureus*, two kinds of MRSA, and *Staphylococcus epidermidis*, and the Black TNDs (MIC = 64 μ g mL⁻¹) had the best antibacterial activity compared with the other TNDs (MIC \geq 128 μ g mL⁻¹). Therefore, the Black TNDs and the Dark TNDs were selected for the next set of antibacterial experiments against MRSA (Figures 2A and S13). To sum up,



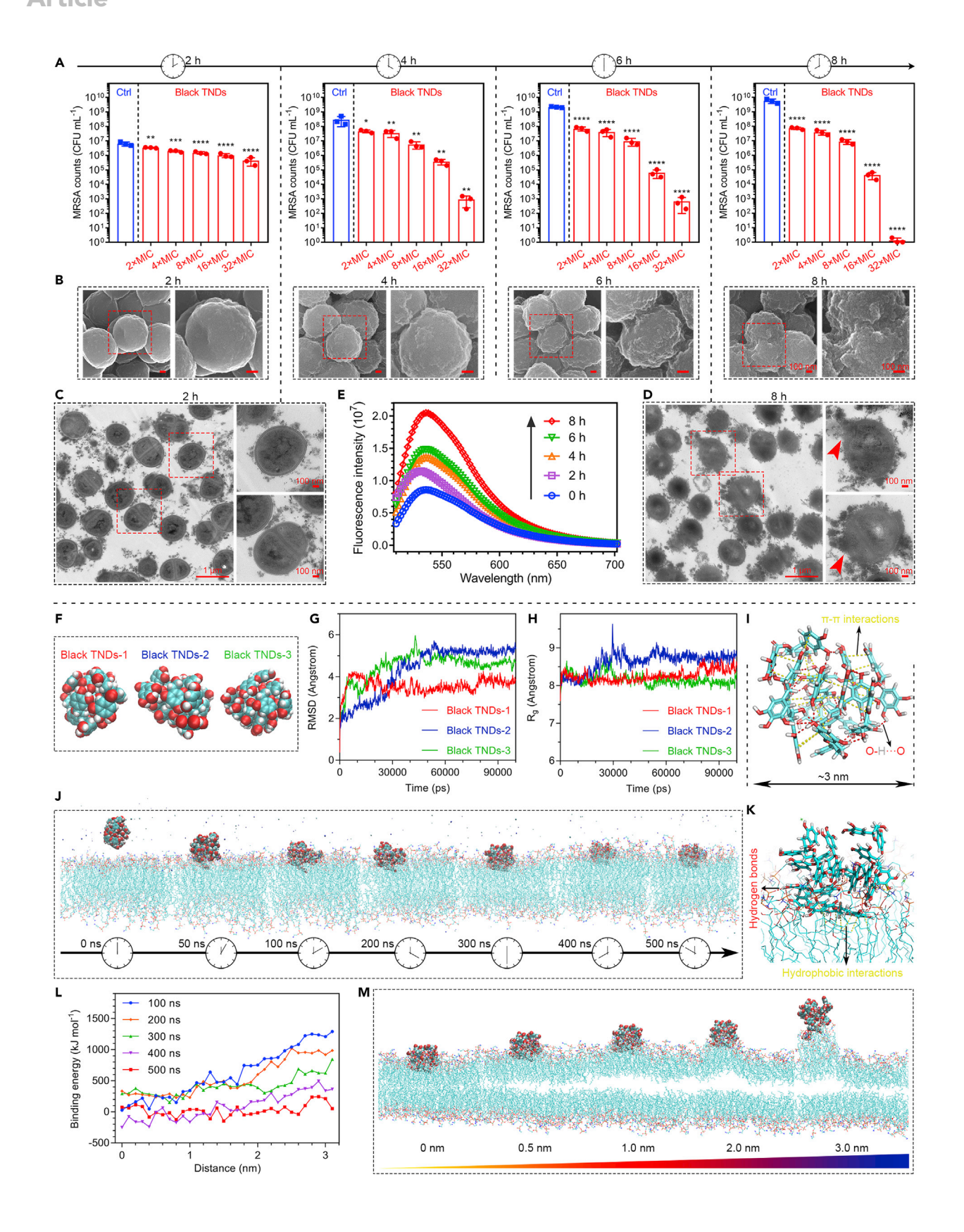






Figure 2. Inactivation kinetics of MRSA treated with Black TNDs and transmembrane process of Black TNDs

(A) Viability of MRSA treated with Black TNDs at various concentrations ($2 \times MIC$, $4 \times MIC$, $8 \times MIC$, $16 \times MIC$, and $32 \times MIC$) in a time-dependent manner (2, 4, 6, and 8 h) and measured by spread plate method.

- (B) SEM images of MRSA treated with Black TNDs in a time-dependent manner (2, 4, 6, and 8 h). Scale bars, 100 nm.
- (C) TEM images of ultrathin sections of MRSA treated with Black TNDs at 2 h. Scale bars, 1 μ m and 100 nm.
- (D) TEM images of ultrathin sections of MRSA treated with Black TNDs at 8 h. Scale bars, 1 μ m and 100 nm.
- (E) Fluorescence intensity of SYTOX Green by MRSA treated with Black TNDs in a time-dependent manner (2, 4, 6, and 8 h).
- (F) Models of Black TND complexes in top three terms using molecular docking.
- (G) RMSD of these models in top three terms to evaluate their stability by MD simulation (100 ns).
- (H) R_{α} profiles of these models in top three terms to evaluate their stability by MD simulation (100 ns).
- (I) Specific model of most stability of Black TNDs by hydrogen bonds (O-H···O, dotted red lines) and π - π interactions (dotted yellow lines).
- (J) Representative configurations of MD simulations at 50, 100, 200, 300, 400, and 500 ns, corresponding to Video S4.
- (K) Specific molecular interactions between Black TNDs and membrane lipid bilayers by hydrogen bonds (dotted red lines) and hydrophobic interactions (dotted yellow lines) in MD simulation at 300 ns.
- (L) Binding energy profiles of Black TND-bacterial membrane composite at different membrane penetration stages (100, 200, 300, 400, and 500 ns) during MD simulation process.
- (M) Tensile MD simulations between Black TNDs and membrane lipid bilayers at different distances (0, 0.5, 1.0, 2.0, and 3.0 nm) at 500 ns, corresponding to Video S5.

Individual data points (n = 3 biologically independent samples) and error bars indicate means \pm standard deviation (SD). Statistical differences between control (Ctrl) and Black TND groups were analyzed by one-way ANOVA and post hoc Dunnett's test (*p < 0.05, **p < 0.01, ***p < 0.001, ****p < 0.0001). Atomic color coding in crystal structure: C, cyan; O, red; H, light gray.

Black TNDs showed optimized antibacterial efficiency, the details of which are described below.

In Figures S1A and S1B, the Black TNDs had a uniform particle size distribution with an average size of 3.19 \pm 0.39 nm, evaluated by the transmission electron microscopy (TEM) imaging and the corresponding statistical analysis. The main components of the Black TNDs (Figure S1C) were eight kinds of tea catechins; the corresponding chemical structures, illustrated in Figure S1D, include (+)-catechin (CA), (-)-epicatechin (EC), (+)-gallocatechin (GC), (-)-epigallocatechin (EGC), (+)-catechin gallate (CG), (-)-epicatechin gallate (ECG), (-)-gallocatechin gallate (GCG), and (-)-epigallocatechin gallate (EGCG). The corresponding compounds in the TNDs were identified using high-performance liquid chromatography coupled with tandem mass spectrometry (HPLC-MS/MS), as shown in Figures S3 and S4 and Data S1. The corresponding details are described in Note S1. Specifically, the Black TNDs had definite mass ratio of eight molecules (CA 29.87%, EC 20.96%, GC 16.19%, EGC 8.84%, CG 5.91%, ECG 4.07%, GCG 7.11%, and EGCG 7.06%), as measured by HPLC-MS/MS in Figures S1C and S5 and Data S1. These eight molecules have common characteristics. In brief, Ring A, Ring B, and Ring E are phenol rings with two or three phenolic hydroxyl groups, while Ring D is a heterocycle, not a phenol ring. Moreover, Ring A has a resorcinol-type arrangement, and Ring B and Ring E have a structural moiety of catechol or three neighboring hydroxyl substituents. The data and corresponding descriptions of the other kinds of TNDs are shown in Figures S2 and S4-S10, Data S1, and Note S2. To sum up, the uniformity of these TNDs and the reproducibility of their composition were excellent. In addition, Fourier transform infrared spectroscopy (Figure S11) and UV-visible spectra (Figure S12) are described in Note S2.

MRSA-killing kinetics of Black TNDs

As shown in Figures 2A and S13, the MRSA-killing kinetics of the Black TNDs and the Dark TNDs in concentrations ranging from 2× MIC to 32× MIC were investigated at specific points in time (2, 4, 6, and 8 h), which showed concentration-dependent and time-dependent positive correlation characteristics. Overall, the antibacterial rates of the Black TNDs were much higher than those of the other TNDs under the same conditions, primarily due to differences in their chemical components and

Matter Article



structures. Specifically, at 2 h the Black TNDs (from 47.17% + 3.51% with $2 \times$ MIC to 93.14% \pm 4.04% with 32 \times MIC) displayed greater bacterial killing efficiency than the Dark TNDs (from 39.27% \pm 3.95% with 2× MIC to 80.41% \pm 6.98% with 32× MIC). Over time, the antibacterial activities increased in the Black TND groups (from 83.91% \pm 3.55% with 2× MIC to 99.99968% \pm 0.00023% [5.50-log reduction] with 32× MIC at 4 h; from 96.79% \pm 0.99% with 2× MIC to 99.999969% \pm 0.000027% [6.51-log reduction] with 32× MIC at 6 h) and the Dark TND groups (from 66.59% \pm 20.82% with 2× MIC to 98.75% \pm 0.53% with 32× MIC at 4 h; from 73.99% \pm 0.58% with 2× MIC to 99.98% \pm 3.72% with 32× MIC at 6 h). Finally, at 8 h, the antimicrobial efficiencies of the Black TNDs (from 98.71% \pm 0.22% with $2 \times$ MIC to 99.99999976% \pm 0.000000010% [9.62-log reduction] with $32 \times$ MIC) were significantly higher than those of Dark TNDs (from 91.94% \pm 1.41% with 2× MIC to 99.99965% \pm 0.00030% [5.46-log reduction] with 32× MIC). Therefore, the Black TNDs were selected for further study because they had the best antibacterial rates among the six kinds of TNDs. Additionally, compared with eight separate molecules in Black TNDs and the mixtures by the same ratio in Black TNDs, the Black TNDs still showed the best antibacterial efficiency (Table S2 and Figure S14), suggesting that the assembled nanostructure had greater advantages than separate small molecules. More details about this are described in Note S3.

As shown in Figure 2B, dynamic changes in the morphologies of the MRSA bacteria incubated with the Black TNDs for 2, 4, 6, and 8 h were observed using scanning electron microscopy (SEM). Obviously, the MRSA bacteria interacting with the Black TNDs for 2 h showed relatively spherical shapes with slightly damaged bacterial membranes compared with the control (Ctrl) group (Figure S15). Additionally, a few Black TNDs adsorbed on the surface of the bacterial membranes, suggesting that the Black TNDs had an apparent interaction with the MRSA membrane and would disrupt the bacterial membrane. Over time, more and more Black TNDs adsorbed on the surface of the bacterial membranes, and the MRSA bacteria gradually became more corrugated, irregular, or even partly lysed, which was consistent with the antibacterial results shown in Figure 2A. Collectively, the degree of bacterial destruction became increasingly serious over time, which was preliminarily attributed to the strong interaction between the Black TNDs and the MRSA membranes.

For further exploration of the detailed changes of the inner structures of MRSA interacting with Black TNDs for 2 h, corresponding TEM images of the ultrathin section are shown in Figure 2C, where the outer membranes of MRSA were relatively regular and completely surrounded by Black TNDs compared with the Ctrl group (in Figure S16). Over time, the corresponding TEM images of MRSA treated with Black TNDs for 8 h (Figure 2D) fully confirmed that the Black TNDs strongly interacted with MRSA membranes and were deeply embedded in the lipid bilayers of MRSA (marked by red arrows). The strong interaction between the Black TNDs and the lipid bilayers of MRSA might result from their interaction (hydrogen bonds and hydrophobic interactions), and the related mechanism will be discussed later. Meanwhile, MRSA membrane permeability was spectrophotometrically measured by examining the uptake of SYTOX Green (Figure 2E), indicating that the Black TNDs induced the gradual permeabilization of the MRSA membranes over time (0–8 h). In brief, the Black TNDs gradually destroyed the whole membrane structure and induced membrane permeabilization to eradicate the bacteria.

Black TND stability analysis

In view of the Black TNDs' average size of ~3.19 nm and eight kinds of molecules (CA 29.87%, EC 20.96%, GC 16.19%, EGC 8.84%, CG 5.91%, ECG 4.07%, GCG 7.11%,





and EGCG 7.06%), simulated models were built using a specific numeric ratio (10 molecules; CA 3, EC 2, GC 2, EGC 1, CG/ECG 1, and GCG/EGCG 1). In the solution system, there was still a certain difference between the state and the conformation from the rigid docking of these molecules to form the Black TNDs. To better understand TND stability and solvent effects in a solution system, based on the lowest-energy principle we performed a 100-ns molecular dynamics (MD) simulation of the models in the top three terms (Figure 2F; Videos S1, S2, and S3).

The root-mean-square deviation (RMSD) approximately showed the relative change in the conformation of the system, which was an important criterion for judging whether the simulation system converged. Therefore, the RMSD was used to determine and judge the balance and stability of the system. The RMSD curves of all Black TND skeletons relative to the simulated initial structures are shown in Figure 2G. The RMSD of the system in the initial state fluctuated greatly due to the adaptation and adjustment of the complex molecules to the changes in the system. After 50 ns, the three systems tended to balance and fluctuate within 1 Å, suggesting that the complex tended to be stable in the solution system. Compared with Black TNDs-2 and Black TNDs-3, Black TNDs-1 had the smallest RMSD and was the most stable. At the same time, the radius of gyration (R_a) , a metric of the size of molecules, characterized the degree of conformational compactness during the MD simulation. The trajectory of the R_q profile demonstrated the stability of the Black TNDs in the dynamic process and explained the tightness of their structure. As shown in Figure 2H, during the initial MD simulation period, due to the solvation and self-adaptation of their structure, the R_{α} profiles of the Black TNDs-2 and the Black TNDs-3 fluctuated greatly, indicating the poor stability of their structures. Moreover, the small molecules in the Black TNDs-2 and the Black TNDs-3 almost underwent disaggregation, which was confirmed by their conformational changes, as shown in Videos S1, S2, and S3, and Figure S17.

By comprehensively comparing the conformational changes of the three systems, the structure of the Black TNDs-1 remained compact during the entire MD simulation process, and there was no sign of disaggregation. Therefore, the Black TNDs-1 (abbreviated as "Black TNDs" below) was selected for the next study on the transmembrane MD simulation. Black TNDs with a simulated size of ~3 nm possessed definite stability due to their abundant hydrogen bonds (O–H···O, dotted red lines) and strong π - π interactions (dotted yellow lines), as shown in Figure 2I. These bonding interactions were formed during the synthesizing process. Notably, the polar branch groups (phenolic groups) in the Black TNDs also played essential roles in membrane attachment and penetration, and the transmembrane activity of the Black TNDs was directly related to their physical mechanism of bacteria-killing activity.

Transmembrane MD simulation of Black TNDs

All-atom MD simulation was performed for the transmembrane process of the Black TNDs to explore molecular interactions between the Black TNDs and the membrane lipid bilayers of *S. aureus*. In Figure 2J and Video S4, the conformational extraction and comparative analysis of the entire process of MD simulations (500 ns) of the Black TND-bacterial membrane complex system are shown. Initially (50 ns), Black TNDs were attached to the surface of the bacterial membrane by binding polar phenolic hydroxyl to hydrophilic lipid heads by forming hydrogen bonds (dotted red lines), as shown in Figure S18. After several hundred nanoseconds, the Black TNDs gradually penetrated the deeper membrane interior and increased the interactions between the benzene rings and the hydrophobic lipid tails through hydrophobic interactions (dotted yellow lines in Figures 2K and S18). After penetration

Matter Article



(500 ns), the Black TNDs completely embedded the lipid bilayer through enhanced interactions and led to a severe disorder in the lipid bilayer (Figure S18). Consequently, these MD simulations showed that the phenolic groups of the Black TNDs gradually anchored the Black TNDs to the lipid bilayers by forming hydrogen bonds and hydrophobic interactions, where the Black TNDs quickly penetrated the lipid bilayers to induce sparser lipid densities, substantial perturbations, and severe deformations of the lipid bilayers (Figure S18), as experimentally validated by the TEM images (Figures 2C and 2D).

To better understand the interaction process, we calculated the profiles of the Black TND-bacterial membrane composite at different membrane penetration stages (Figure 2L). The lower the binding energy, the more stable the binding molecules in the Black TNDs.^{23,24} As shown in Figure 2L, the gradual decrease in binding energy over time (100-500 ns) indicated that the binding stability was stronger when the Black TNDs gradually penetrated into the bacterial membrane, thereby preventing the Black TNDs from falling off and ensuring the smooth progress of the membrane perforation process. To visually verify the disruptive extraction of the lipid molecules, we conducted tensile dynamic simulations at 500 ns (Figure 2M and Video S5), which suggested that the pulling process of the Black TNDs caused part of the lipid bilayers to be taken out. With the increase in distance (0-3 nm) between the Black TNDs and the bacterial membrane, the Black TNDs continuously dragged on the bacterial membrane and vigorously extracted the phospholipid molecules from the lipid bilayers, which largely resulted from their hydrogen bonds and hydrophobic interactions (Figure S19). As a result, the Black TNDs caused fluctuations, perturbations, and deformations of the lipid bilayers due to the strong dragging forces, thus leading to the loss of cell membrane integrity. In summary, the strong interactions (hydrogen bonds and hydrophobic interactions) between the Black TNDs and the phospholipid bilayer guaranteed the smooth accomplishment of the transmembrane MD simulation of the Black TNDs. Importantly, this antibacterial mechanism based on the physical damage to bacterial membrane had a low probability of developing bacterial resistance. 23,24

Proteomics of MRSA treated with Black TNDs

To comprehensively reveal the biologically antibacterial mechanism by the Black TND treatment, we conducted a quantitative proteomic approach based on tandem mass tag technology to explore the changes of protein abundance in MRSA bacteria without and with Black TND treatment. In Figure 3A, a volcano plot of the proteomics indicates 1,089 identified proteins. The 60 downregulated proteins (cutoff value of 0.5-fold for expressed variation, p < 0.05) and the 98 upregulated proteins (cutoff value of 2.0-fold for expressed variation, p < 0.05) implied a diverse variety of biological changes in MRSA owing to Black TND treatment. These differential proteins in MRSA are illustrated in the heatmap in Figure S20 and in Table S3, demonstrating good intragroup and intergroup parallelism.

To clearly identify the specific biological changes in MRSA, we commonly classified all differential proteins into three classes (biological process, molecular function, and cellular component) based on gene ontology (GO) classification, as shown in Figure 3B and Tables S4 and S5, where the top 20 terms are enriched and displayed. Obviously the most significant changes of the differential proteins focused on the bacterial membrane in the cellular component, including "membrane, "intrinsic component of membrane," "integral component of membrane," and "membrane part." The altered MRSA membranes using GO enrichment analyses (Figure 3B)



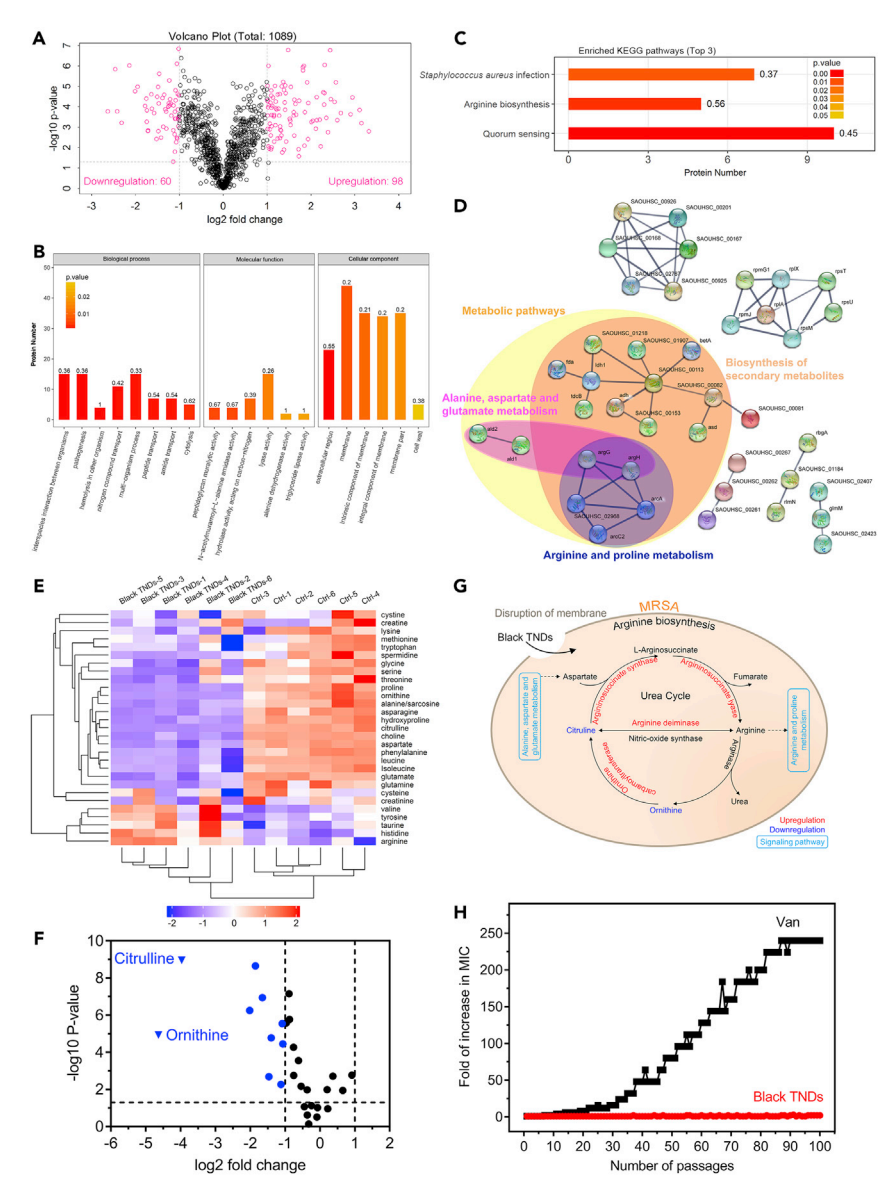


Figure 3. Proteomics and targeted metabolomics of amino acids of MRSA treated with Black TNDs without detectable mutant development

(A) Volcano plot of 1,089 identified proteins, including 60 downregulated proteins (cutoff value of 0.5-fold for expressed variation, p < 0.05) and 98 upregulated proteins (cutoff value of 2-fold for expressed variation, p < 0.05) in MRSA by Black TND treatment (n = 3 biologically independent samples).

- (B) GO classifications (Biological process, Molecular function, and Cellular component) of all differential proteins of MRSA treated with Black TNDs and enriched GO terms in top 20.
- (C) KEGG annotations of identified proteins underlying pathways and processes, and enriched KEGG pathways in the top three terms.
- (D) PPI networks of these proteins classified by signaling pathways.
- (E) Heatmap analysis of 29 identified amino acids of MRSA treated with Black TNDs compared with $Ctrl\ (n=6\ biologically\ independent\ samples).$
- (F) Volcano plot of 29 identified amino acids, including 10 downregulated amino acids (cutoff value of 0.5-fold for expressed variation, p < 0.05) and no upregulated amino acids (cutoff value of 2-fold for expressed variation, p < 0.05) in MRSA by Black TND treatment.
- (G) Scheme of subcellular localization in arginine biosynthesis signaling pathway by combining proteomics with targeted metabolomics (red color: upregulation; blue color: downregulation; wireframe: signaling pathway).
- (H) Monitoring of drug-resistant development of MRSA after exposure to Black TNDs and Van at sub-MIC concentrations over 100 serial passages.





were in good agreement with the morphological changes of the MRSA membrane in experimental observation and theoretical simulation (Figure 2).

Various kinds of protein components in bacterial membranes play important roles in many cellular processes. Therefore, the interplay between the Black TNDs and the bacterial membrane caused a series of metabolic changes in bacteria. Furthermore, the identified proteins underlying the signaling pathways were explored by the Kyoto Encyclopedia of Genes and Genomes (KEGG) annotations (Table S6). As shown in Figure 3C, the top three terms of the enriched KEGG pathways are "quorum sensing," "arginine biosynthesis," and "Staphylococcus aureus infection." Among these, the arginine biosynthesis signaling pathway had the highest proportion of differential proteins (56%, p < 0.05). In the arginine biosynthesis signaling pathway, amino acid metabolism is important for bacterial nutritional homeostasis and intracellular metabolic pathways. Furthermore, protein-protein interaction (PPI) network analysis (Figure 3D) in the proteomics further confirmed that the differential proteins had a close correlation with the intracellular metabolic pathways, including "biosynthesis of secondary metabolites," "alanine, aspartate and glutamate metabolism," and "arginine and proline metabolism." Collectively, the results of the KEGG annotation and the PPI network fully indicated the significant alteration of the amino acid metabolism in MRSA by Black TND treatment.

Targeted metabolomics of amino acids and biologically antibacterial

Guided by the proteomics results, to locate the specific target of amino acid metabolism in MRSA by Black TND treatment, the targeted metabolomics identified metabolic changes of 29 amino acids, as shown in Figure 3E and Table S7. Specifically, the heatmap showed good intragroup and intergroup parallelism when comparing the Black TND groups to the Ctrl groups (n = 6). Furthermore, the volcano plots of the targeted metabolomics demonstrated 29 identified amino acids in Figure 3F (for more detailed data see Figure S21). The ten downregulated amino acids (cutoff value of 0.5-fold for expressed variation, p < 0.5) and lack of upregulated amino acids (cutoff value of 2.0-fold for expressed variation, p < 0.5) suggested that the Black TNDs suppressed the metabolism process of the amino acids in MRSA. Citrulline (0.064-fold, p < 10^{-9}) and ornithine (0.040-fold, p < 10^{-5}) had the most prominent downregulation. To systematically seek the accurate target of the Black TNDs against MRSA, we evaluated joint signaling pathways by combining proteomics with targeted metabolomics. Among these, the arginine biosynthesis signaling pathway (Figure S22) was the most prominent and was in good agreement with the enriched KEGG pathways, as shown in Figure 3C.

The subcellular localization in Figure 3G corresponding to the arginine biosynthesis signaling pathway (Figure S22) indicated that the most obvious change occurred in the biological process of the "urea cycle," where the two amino acids (citrulline and ornithine) of the most prominent downregulation were closely related to the two kinds of highly upregulated proteins (ornithine carbamoyltransferase and argininosuccinate synthase). Accordingly, the most important biochemical reactions were analyzed and are shown in detail in Figures S23 and S24. In Figure S23A, ornithine carbamoyltransferase (5.80-fold, p < 10^{-4} , Figure S23B) can catalyze ornithine (0.040-fold, p < 10^{-5} , Figure S23C) to produce citrulline (0.064-fold, p < 10^{-9} , Figure S23D). Additionally, as shown in Figure S24A, argininosuccinate synthase (5.47-fold, p < 10^{-4} , Figure S24B) can catalyze and consume citrulline (0.064-fold, p < 10^{-9} , Figure S24C) and adenosine triphosphate (ATP, 0.15-fold, p < 10^{-3} , Figure S24D), and the ATP levels in MRSA were measured by a bacterial ATP assay





kit. In brief, proteomics and targeted metabolomics collectively revealed that the accurate target of the Black TNDs against MRSA was the disruption of the biochemical reactions of ornithine and citrulline in the "urea cycle" in the arginine biosynthesis signaling pathway of MRSA.

In Figure 3H, the drug-resistant development of MRSA after exposure to the Black TNDs and clinically used vancomycin (Van) at sub-MIC concentrations over 100 serial passages was monitored. The Van group had a 240-fold increase in drug-resistant development, but the Black TND group killed MRSA without detectable resistant development. By comprehensively analyzing the above results, the antibacterial mechanism of Black TNDs against MRSA had two critical aspects: (1) physical transmembrane interactions to destroy the bacterial membrane and (2) biologically specific targets to disrupt the biochemical synthesis of citrulline and ornithine. Consequently, the low probability of developing bacterial resistance to the Black TNDs was ascribed to this new antibacterial mechanism, based on their physical damage and biological target. Importantly, this mechanism provides a valuable idea for exploiting new antibacterial drugs without detectable drug-resistant development.

Cytocompatibility of Black TNDs

The viability of the alveolar cells and macrophages treated with Black TNDs ranging from 128 to 2,048 μg mL⁻¹ on days 1, 3, and 7 is shown in Figure S25. Overall, the Black TND groups at various concentrations for different incubation times had no significant cytotoxicity to alveolar cells (Figure S25A) and macrophages (Figure S25B) compared with the Ctrl group, suggesting that the Black TNDs showed excellent cytocompatibility of alveolar cells and macrophages. Although the cell viability of Black TNDs at high concentrations (1,024 and 2,048 μg mL⁻¹) on day 1 was not good, the cytocompatibility gradually became better over time. Besides, the Black TNDs at high concentrations (from 2,048 to 16,384 μg mL⁻¹) for 1 day exhibited obvious cytotoxicity (Figure S26), whereby the maximum resistance dose of alveolar cells to Black TNDs was approximately 16,384 μg mL⁻¹.

Antiviral mechanism of Black TNDs

The antiviral activities of Black TNDs at different concentrations were assessed by the H1N1 virus titers with a 50% tissue culture infective dose (TCID $_{50}$) assay. As shown in Figure 4A, the H1N1 virus titers treated with Black TNDs exhibited an obvious and continuous reduction in a concentration-dependent manner. Specifically, the virus titers at 24 h post infection in the Black TND groups (128, 256, and 512 μg mL $^{-1}$) were 3.92, 2.85, and 1.76 log_{10} TCID $_{50}$ mL $^{-1}$, respectively, which were significantly less than those (5.45 log_{10} TCID $_{50}$ mL $^{-1}$) in the Ctrl group. Furthermore, the antiviral efficiency of Black TNDs was also confirmed by the suppression of H1N1 virus replications (Figure 4B). The relative levels of nucleoprotein (NP) RNA expression in the three Black TND groups (less than 13%) were obviously lower than those in the Ctrl group, which were determined by qRT-PCR.

To explore the antiviral mechanism of Black TNDs against H1N1, we first measured the H1N1 neuraminidase (NA) activities because NA is the most important and major target of antiviral drugs. As shown in Figure 4C, Black TNDs prominently inhibited NA activities, and the inhibitory effects of Black TNDs continuously increased as their concentration increased. Furthermore, the morphologies of the H1N1 viruses coincubated with the Black TNDs were observed by SEM and TEM (Figure 4D). Obviously, a mass of Black TNDs were adsorbed on the surface of the H1N1 viruses, and the H1N1 viruses in the Black TND groups became irregular and damaged (marked by red arrows) compared with those in the Ctrl group.



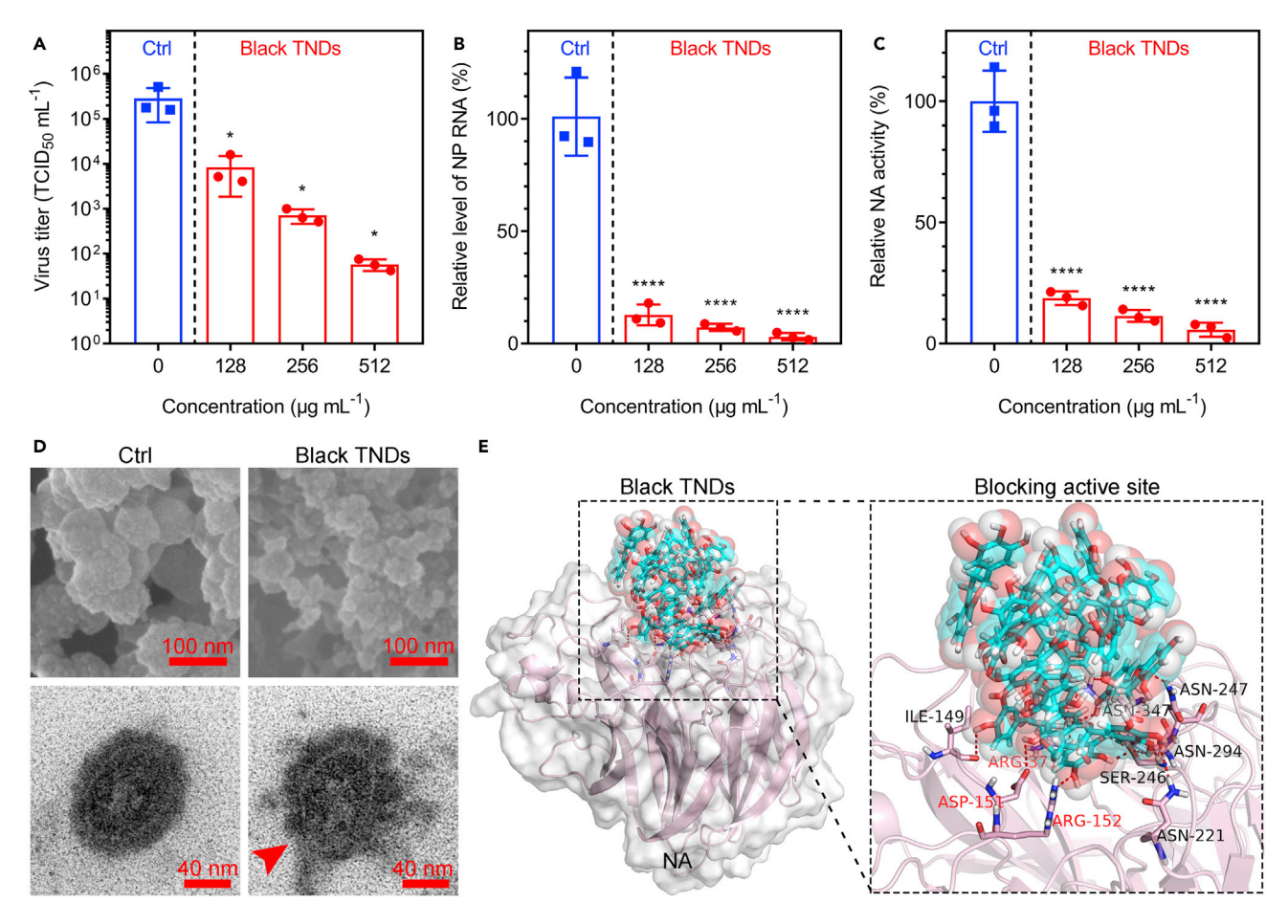


Figure 4. Antiviral mechanism of Black TNDs

- (A) H1N1 virus titers by TCID₅₀ assay by treatment with Black TNDs at various concentrations (128, 256, and 512 µg mL⁻¹).
- (B) Relative level of NP RNA by treatment with Black TNDs at various concentrations (128, 256, and 512 μg mL⁻¹).
- (C) Relative NA activity by treatment with Black TNDs at various concentrations (128, 256, and 512 µg mL⁻¹).
- (D) SEM images (scale bars, 100 nm) and TEM images (ultrathin sections; scale bars, 40 nm) of H1N1 treated with Black TNDs at 24 h.
- (E) Molecular docking between Black TNDs and NA by dense hydrogen-bond network.

Individual data points (n = 3 biologically independent samples) and error bars indicate means \pm SD. Statistical differences between Ctrl and Black TNDs groups were analyzed by ANOVA and post hoc Dunnett's test (*p < 0.05, ****p < 0.0001). Atomic color coding in crystal structure: C, cyan; O, red; H, light gray.

The tight interaction between Black TNDs and H1N1 viruses might suppress NA activities by binding the active sites. Therefore, a molecular docking between the Black TNDs and NA was performed. The NA active site of the H1N1 virus is highly flexible and locates between loops 150 and 430.²⁵ As shown in Figure S27, the NA active site pocket was surrounded by nine key residues (ASP151, ARG152, ARG371, ILE149, ASN221, SER246, ASN247, ASN294, and ASN347). According to the molecular docking calculations, the NA active site was docked with Black TNDs (Figure S28), which was preliminarily indicative of a tight interaction with each other. To further explore the details of their binding force, we used a binding mode based on the lowest-energy principle was used for visual analysis. As shown in Figure 4E, Black TNDs were inserted into the active site pocket because the size of the Black TNDs spatially matched the active site pocket, facilitating the formation of larger contact surfaces. The abundant surface hydroxyl groups of the Black TNDs provided sufficient hydrogen-bond receptors when interacting with the NA active site pocket.





Meanwhile, the nine key residues around the active site pocket served as hydrogen-bond donors. Therefore, abundant hydrogen-bond interactions (dotted red lines) were tightly formed between the Black TNDs and the nine key residues. Notably, the key binding residues (marked by red colors: ASP151, ARG152, and ARG371) are central to their binding stability. At the same time, the Black TNDs had double hydrogen-bond interactions with many residues, such as ARG371, ASN347, and SER246.

The dense hydrogen-bond network between the Black TNDs and the active site pocket blocked the NA active site, enabling the Black TNDs to effectively inhibit NA activity. This antiviral mechanism of the Black TNDs by targeting the NA active site pocket provided a pharmacological understanding of NA inhibitors through strong hydrogen-bond interactions. This strategy also provided fundamental insights into the development of antiviral therapeutics.

In vivo biosafety of Black TNDs in piglets

To further confirm the biosafety of the synthesized TNDs, we selected pigs as an animal model for toxicological study because they have closer similarity with humans than mice, and their anatomy and physiology closely resemble those of humans. 26,27 Additionally, the most common drug-delivery methods in toxicological studies include intravenous injection (i.v.) and oral administration (OA).²⁶ Moreover, the method of aerosol therapy (AT) in the pneumonia model was widespread. Therefore, as illustrated in Figure 5A, the three drug-delivery methods (i.v., AT, and OA) were used on the piglets for 14 days for the biosafety evaluation, including hematology, urinalysis, renal function, hepatic function, anaphylactic reaction measurements, and histology of major organs. In Figure 5B, the hematology results of the Ctrl and Black TND groups showed no significant differences (p > 0.05), and all data were within the corresponding normal scope (marked by dashed lines), including hematocrit (HCT), hemoglobin (HGB), mean corpuscular hemoglobin (MCH), mean corpuscular hemoglobin concentration (MCHC), mean corpuscular volume (MCV), mean platelet volume (MPV), platelet count (PLT), red blood cell count (RBC), red cell distribution width (RDW), and white blood cell count (WBC). Moreover, urinalysis data (Figure 5C) showed that all items were normal (the dash represents a negative result), including bilirubin (BIL), blood (BLD), glucose (GLU), ketone (KET), nitrite (NIT), protein (PRO), urobilinogen (URO), ascorbic acid (Vc), and WBC. In addition, biochemical analyses of the hepatic function (Figure 5D) and the renal function (Figure 5E) indicated no significant differences (p > 0.05) between the Ctrl and the Black TND groups, including blood urea nitrogen (BUN), creatinine (CRE), uric acid (UA), albumin (ALB), alkaline phosphatase (ALP), alanine transaminase (ALT), aspartate transaminase (AST), cholinesterase (CHE), direct bilirubin (DBIL), glutamyl transpeptidase (GGT), total bile acid (TBA), total bilirubin (TBIL), and total protein (TP). Additionally, the levels of C-reactive protein, immunoglobulin E (IgE), IgG, and histamine in the piglets demonstrated that the Black TNDs did not induce anaphylactic reaction (Figure 5F). Moreover, the corresponding histological analyses of the major organs (heart, liver, spleen, lung, kidney, and brain) using hematoxylin-eosin (H&E) staining (Figure 5G) showed no signs of organ damage. In summary, these results further confirmed that the Black TNDs had excellent biosafety in piglets and great potential for clinical therapy for MRSA-induced pneumonia.

Drug compatibility of Black TNDs

Inspired by Chinese medicinal formula compatibility, three common Chinese medicine monomer molecules were selected for screening of optimized synergistic antiviral and antibacterial collocation, namely Ber, Que, and Lut. The corresponding



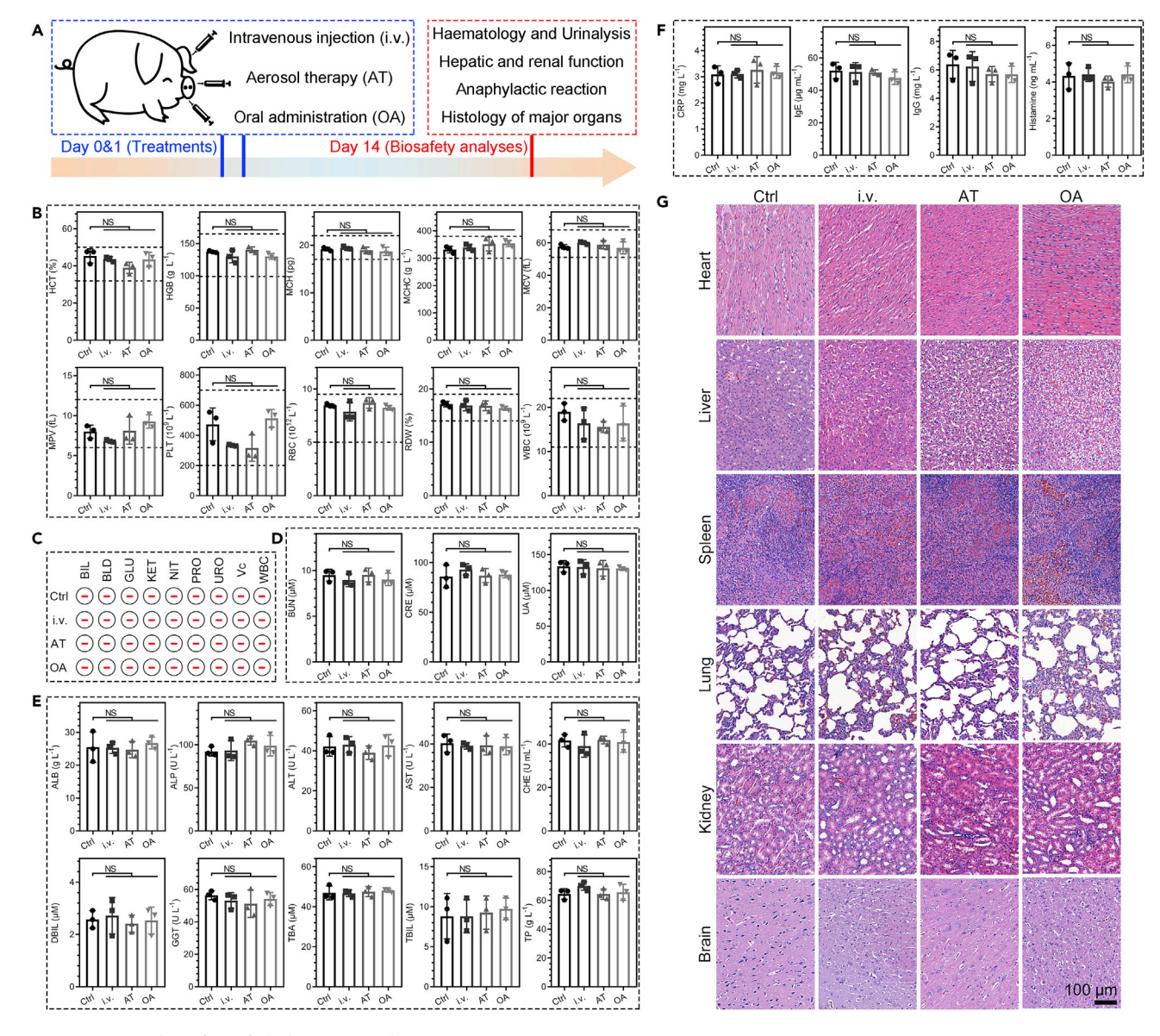


Figure 5. In vivo biosafety of Black TNDs in piglets

- (A) Schematic illustration of three treatments (i.v., AT, and OA) by Black TNDs in piglets.
- (B) Hematology of Ctrl, i.v., AT, and OA groups on day 14, including HCT, HGB, MCH, MCHC, MCV, MPV, PLT, RBC, RDW, and WBC. Lines of dashes mark corresponding normal scope.
- (C) Urinalysis of Ctrl, i.v., AT, and OA groups on day 14, including BIL, BLD, GLU, KET, NIT, PRO, URO, Vc, and WBC (dash in circle represents a negative result).
- (D) Biochemical analyses of renal function (BUN, CRE, and UA) of Ctrl, i.v., AT, and OA groups on day 14.
- (E) Biochemical analyses of hepatic function (ALB, ALP, ALT, AST, CHE, DBIL, GGT, TBA, TBIL, and TP) of Ctrl, i.v., AT, and OA groups on day 14.
- (F) Anaphylactic reactions (C-reactive protein, IgE, IgG, and histamine) of Ctrl, i.v., AT, and OA groups on day 14.
- (G) Histological analyses of major organs (heart, liver, spleen, lung, kidney, and brain) of Ctrl, i.v., AT, and OA groups on day 14 using H&E staining. Scale bar, 100 μ m.

Individual data points (n = 3 biologically independent samples) and error bars indicate means \pm SD. Statistical differences were analyzed by one-way ANOVA and post hoc Tukey's test (NS, not significant, p > 0.05).

structures of these three molecules are illustrated in Figure S29. As shown in Figure 6A, these molecules at the same concentrations (64 μ g mL⁻¹) had certain antiviral activities. To comprehensively identify the optimized synergistic antiviral molecules, we integrated the Black TNDs at different concentrations (128, 256, and





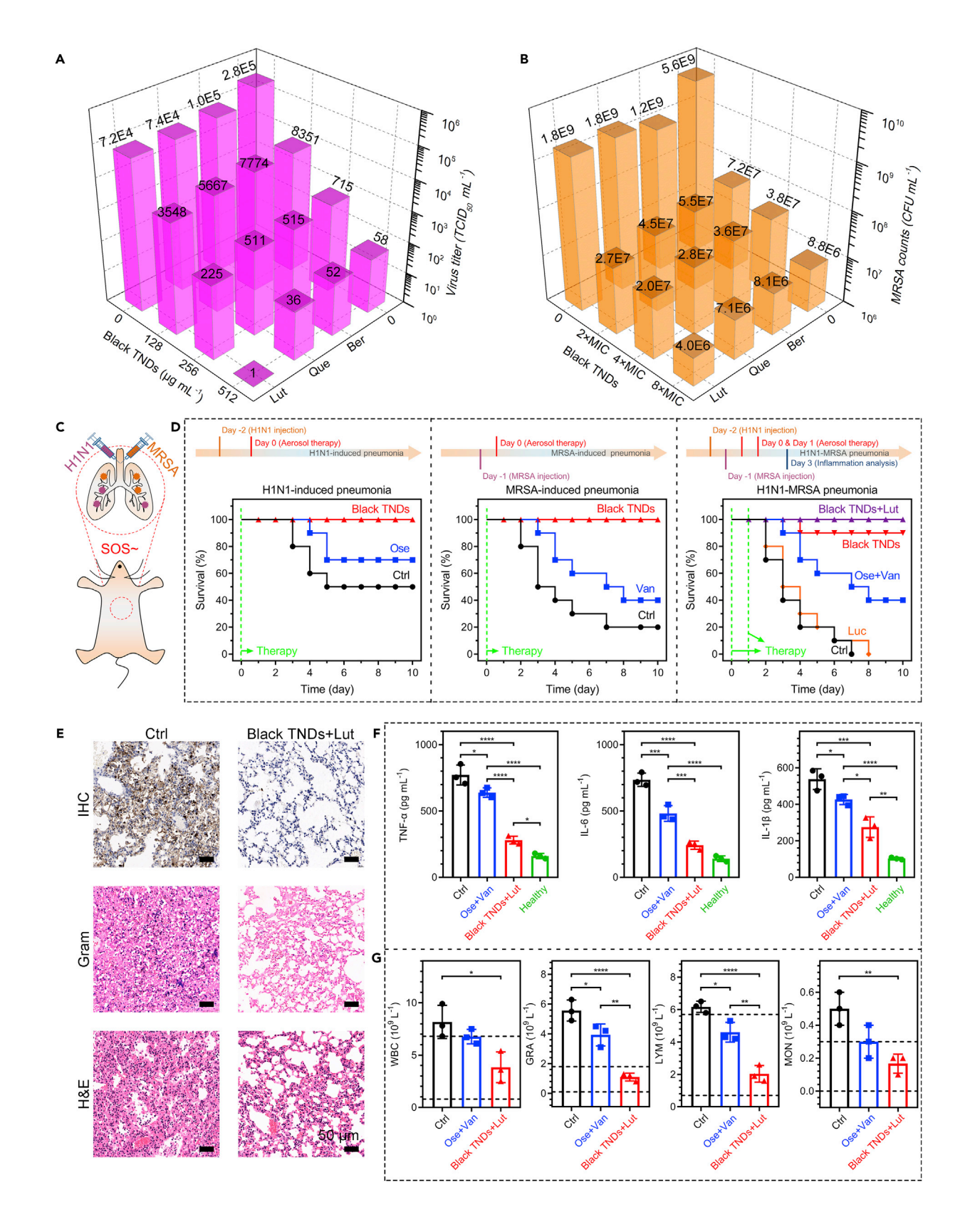






Figure 6. Drug compatibility of Black TNDs and lethal H1N1-MRSA pneumonia model

(A) Synergistic antiviral activities by combining different molecules (Ber, Que, and Lut) with Black TNDs at different concentrations (128, 256, and 512 μ g mL⁻¹).

- (B) Synergistic antibacterial activities by combining different molecules (Ber, Que, and Lut) with Black TNDs at different concentrations (128, 256, and $512 \, \mu g \, mL^{-1}$).
- (C) Schematic illustration of lethal H1N1-MRSA pneumonia model.
- (D) Timelines and mouse survival curves of H1N1-induced pneumonia, MRSA-induced pneumonia, and H1N1-MRSA pneumonia over time (n = 10 mice in each group).
- (E) IHC staining, Gram staining, and H&E staining of lungs of mice in Ctrl and Black TNDs + Lut groups on day 1, day 3, and day 7. Scale bars, 50 μ m. (F) Levels of inflammatory factors (TNF- α , IL-6, and IL-1 β) in lungs.
- (G) Number of inflammatory corpuscles (GRA, LYM, MON, and WBC) in MRSA-induced pneumonia in blood on day 7.

Individual data points (n = 3 biologically independent samples) and error bars indicate means \pm SD. Statistical differences were analyzed by one-way ANOVA and post hoc Tukey's test (*p < 0.05, **p < 0.01, ***p < 0.001, ****p < 0.0001).

 $512\,\mu g\,m L^{-1}$) with Ber, Que, and Lut, respectively. Obviously, the combination of Lut and Black TNDs had the best synergistic antiviral effect. Similarly, as shown in Figure 6B, the optimal synergistic antibacterial cooperation was still Lut and Black TNDs. Specifically, all of the three monomer molecules with the same MIC (64 $\mu g\,m L^{-1}$) against MRSA had different synergistic antibacterial activities with Black TNDs at different concentrations (2× MIC, 4× MIC, and 8× MIC), whereby the Lut was the best synergistic antibacterial molecule. In summary, the optimized synergistic antiviral and antibacterial combination was Black TNDs + Lut, and compatible herbal medicines were chosen for subsequent animal experiments.

Lethal H1N1-MRSA pneumonia model

The three animal models of H1N1-induced pneumonia, MRSA-induced pneumonia, and H1N1-MRSA pneumonia are schematically illustrated in Figures 6C and 6D. In brief, H1N1 viruses and MRSA bacteria were intratracheally introduced to cause lethal pneumonia, and bacterial coinfection was performed after 1 day of viral infection. As shown in Figure 6D, for H1N1-induced pneumonia, the Black TND group (100%, n = 10 mice) had the highest survival rate when compared with the Ctrl group (50%, n = 10 mice) and the group administered the clinical antiviral drug oseltamivir (Ose, 70%, n = 10 mice). For MRSA-induced pneumonia, the infected mice in the Ctrl group had only a 20% survival rate on day 10, whereas the mouse survival rate was significantly promoted with the Van (40% survival rate) and Black TND (100% survival rate) treatments. For lethal H1N1-MRSA pneumonia, the infected mice in the Ctrl group had a 20% survival rate on day 4 and up to 100% mortality on day 7, but the mouse survival rate was dramatically improved with aerosol therapies using Black TNDs and Black TNDs + Lut. Specifically, the mice administered Ose + Van showed a limited therapeutic effect with a 40% survival rate at 10 days, while the Black TNDs and Black TNDs + Lut groups had 90% and 100% survival rates, respectively, over 10 days.

Immunohistochemical (IHC) staining exhibited large amounts of H1N1 viral antigens in the Ctrl group on day 3 (Figure 6E, brown color). Comparatively, the negligible viral antigens in the Black TNDs + Lut group confirmed the excellent antiviral activity of Black TNDs + Lut *in vivo*. Additionally, many bacteria (violet color) stained by Gram staining in the Ctrl group indicated severe bacterial coinfection in the lungs on day 3, whereas Black TNDs + Lut showed effective antibacterial activity *in vivo*. Meanwhile, histological analysis of the lungs using H&E staining was conducted on day 3 to evaluate the pulmonary inflammation after H1N1-MRSA coinfection, as shown in Figure 6E. The infected mice in the Ctrl group displayed widespread loss of aerated lung in tissue solidification and obvious signs of neutrophilic pneumonia associated with the H1N1-MRSA coinfection. Moreover, the number of neutrophils significantly increased in the Ctrl group, revealing the massive infiltration and recruitment of neutrophils in the infected lungs. Comparatively, the infected mice treated with Ose + Van showed moderate levels of





neutrophil infiltration in the lung. Remarkably, the infected mice treated with the Black TNDs + Lut showed the best preservation of the alveolar structure and the lowest levels of neutrophil infiltration (Figure 6E), preliminarily indicating that AT using Black TNDs + Lut had much better therapeutic effects for H1N1-MRSA pneumonia than clinical therapy using Ose + Van.

Calming the cytokine storm was important for decreasing the mortality of lethal H1N1-MRSA pneumonia. Overall, the Black TNDs + Lut remarkably inhibited the production of inflammatory factors (tumor necrosis factor α [TNF- α], interleukin-6 [IL-6], and IL-1 β) in the lungs, as shown in Figure 6F. Compared with the Ctrl group, the Ose + Van group exhibited a limited anti-inflammatory therapeutic effect, suggesting that Black TNDs + Lut had a greater advantage as an anti-inflammatory agent than Ose + Van.

In summary, AT using the Black TNDs + Lut effectively reduced the inflammatory factors and pulmonary neutrophil accumulations in the alveolar spaces, simultaneously minimizing neutrophil-mediated pulmonary damage. The high mortality in lethal H1N1-MRSA pneumonia was typically mediated by lung damage due to excess inflammation except for the pathogenic activity by H1N1 and MRSA burdens. Furthermore, the inflammatory response in acute lung injury was closely related to excessive oxidative stress, inducing oxidative damage.²⁸ Thus, anti-inflammation by antioxidative therapy was central to reducing the lethality of pneumonia and restoring lung homeostasis. Besides rapid H1N1 and MRSA clearance, the Black TNDs + Lut possessed anti-inflammatory effects due to their antioxidant capacity $(4 \text{ mmol g}^{-1} \text{ compared with trolox})$, as shown in Figure S30. Moreover, in Figure 6G, the corresponding inflammatory corpuscles, including granulocyte (GRA), lymphocyte (LYM), monocyte (MON), and WBC, were evaluated in cases of H1N1-MRSA pneumonia in the blood on day 3. Obviously, the number of inflammatory corpuscles in the Black TNDs + Lut group within the corresponding normal scope (marked by dashed lines in Figure 6G) was significantly lower than those in the Ctrl and Ose + Van groups, suggesting that the Black TNDs suppressed excess inflammationinduced tissue damage in homeostasis.

Notably, the pharmaceutical dynamics of Black TNDs *in vivo* was through the renal filtration pathway. As shown in Figure S31 and Data S1, the signals of tea catechins were detected in mouse urine by HPLC-MS/MS 24 h after aerosol treatment by Black TNDs. This result indicated that these Black TNDs could be efficiently filtered into the mouse urine through kidney clearance because their size (~3 nm) was below the glomerular filtration cutoff (~5.5 nm). The renal filtration pathway of Black TNDs could minimize their nonspecific accumulation in the reticuloendothelial system and potential toxicity. Furthermore, no histological toxicology (major organs included heart, liver, spleen, lung, and kidney in Figures S32A and S32B) on day 14 and day 28 by H&E staining and the normal hematology results (the corresponding normal scope was marked by dashed lines in Figure S32C) on day 28 after the Black TNDs + Lut treatment in the lethal H1N1-MRSA pneumonia model was confirmed, suggesting long-term biosafety of this treatment.

Conclusion

This work described a therapeutic strategy of material-herbology for lethal H1N1-MRSA pneumonia by combining Black TNDs with Lut. Specifically, the synthesized Black TNDs composed of tea catechins showed highly effective antibacterial and antiviral activity. The antibacterial mechanism against MRSA consisted of physical transmembrane interaction and the inhibition of amino acid metabolism, and the antiviral mechanism against H1N1 blocked the NA active sites. *In vivo* results





showed that Black TNDs had excellent biosafety in piglets, and by combining Black TNDs with Lut the optimized synergistic AT exhibited greater advantage against lethal H1N1-MRSA pneumonia than the reported clinical therapy, owing to the rapid clearance of H1N1 and MRSA as well as the antioxidant-related anti-inflammatory effect. Hence, this strategy may bring a safe and effective alternative to currently clinical therapy against lethal H1N1-MRSA pneumonia through material-herbology.

EXPERIMENTAL PROCEDURES

Resource availability

Lead contact

Further information and requests for materials should be directed to and will be fulfilled by the lead contact, Shuilin Wu, shuilinwu@tju.edu.cn.

Materials availability

This study did not generate new unique reagents.

Data and code availability

The data used to support the findings of this study are available from the corresponding author upon request.

Experimental procedures are described in detail in supplemental information.

SUPPLEMENTAL INFORMATION

Supplemental information can be found online at https://doi.org/10.1016/j.matt. 2021.07.001.

ACKNOWLEDGMENTS

This work is jointly supported by the China National Funds for Distinguished Young Scientists (no. 51925104) and the National Natural Science Foundation of China (nos. 51671081 and 51871162) and by the Natural Science Fund of Hubei Province (2018CFA064). The authors would like to thank State Key Laboratory of Agricultural Microbiology, College of Veterinary Medicine, Huazhong Agricultural University and Laboratory Animal Center, Huazhong Agriculture University for the support of viral experiments.

AUTHOR CONTRIBUTIONS

J.L., Z.Z., X.L., and S.W. conceived and designed the concept of the experiments. J.L. and Z.Z. synthesized the materials and conducted the material characterizations. J.L., X.L., and S.W. analyzed the experimental data and wrote the manuscript. X.L., Y.Z., C.L., Z.C., K.W.K.Y., H.Z., J.Z., Z.L., S.Z., Y.L., X.W., and S.W. provided important experimental insights. All authors discussed, commented on, and agreed on the manuscript.

DECLARATION OF INTERESTS

S.W., J.L., and X.L. have submitted a China patent application (No. 202010229901.3), which contains the fabrication of the technique utilized in this paper. The authors declare no other competing interests.

Received: February 8, 2021 Revised: June 11, 2021 Accepted: June 30, 2021 Published: July 27, 2021





REFERENCES

- Iuliano, A.D., Roguski, K.M., Chang, H.H., Muscatello, D.J., Palekar, R., Tempia, S., Cohen, C., Gran, J.M., Schanzer, D., Cowling, B.J., et al. (2018). Estimates of global seasonal influenza-associated respiratory mortality: a modelling study. Lancet 391, 1285–1300.
- Jamieson, A.M., Pasman, L., Yu, S., Gamradt, P., Homer, R.J., Decker, T., and Medzhitov, R. (2013). Role of tissue protection in lethal respiratory viral-bacterial coinfection. Science 340, 1230–1234.
- 3. McCullers, J.A. (2014). The co-pathogenesis of influenza viruses with bacteria in the lung. Nat. Rev. Microbiol. 12, 252–262.
- Vaillancourt, M., and Jorth, P. (2020). The unrecognized threat of secondary bacterial infections with COVID-19. mBio 11, e01806e01820.
- Zhou, F., Yu, T., Du, R., Fan, G., Liu, Y., Liu, Z., Xiang, J., Wang, Y., Song, B., Gu, X., et al. (2020). Clinical course and risk factors for mortality of adult inpatients with COVID-19 in Wuhan, China: a retrospective cohort study. Lancet 395, 1054–1062.
- Chertow, D.S., and Memoli, M.J. (2013). Bacterial coinfection in influenza a grand rounds review. JAMA 309, 275–282.
- MacLean, R.C., and San Millan, A. (2019). The evolution of antibiotic resistance. Science 365, 1082–1083.
- 8. Chellat, M.F., Raguž, L., and Riedl, R. (2016). Targeting antibiotic resistance. Angew. Chem. Int. Ed. 55, 6600–6626.
- Smith, P.A., Koehler, M.F.T., Girgis, H.S., Yan, D., Chen, Y., Chen, Y., Crawford, J.J., Durk, M.R., Higuchi, R.I., Kang, J., et al. (2018). Optimized arylomycins are a new class of Gram-negative antibiotics. Nature 561, 189–194.

- Baym, M., Stone, L.K., and Kishony, R. (2016). Multidrug evolutionary strategies to reverse antibiotic resistance. Science 351, aad3292.
- 11. Abdelmohsen, U.R., Balasubramanian, S., Oelschlaeger, T.A., Grkovic, T., Pham, N.B., Quinn, R.J., and Hentschel, U. (2017). Potential of marine natural products against drugresistant fungal, viral, and parasitic infections. Lancet Infect. Dis. 17, e30–e41.
- Seiple, I.B., Zhang, Z., Jakubec, P., Langlois-Mercier, A., Wright, P.M., Hog, D.T., Yabu, K., Allu, S.R., Fukuzaki, T., Carlsen, P.N., et al. (2016). A platform for the discovery of new macrolide antibiotics. Nature 533, 338–345.
- Tu, Y. (2011). The discovery of artemisinin (qinghaosu) and gifts from Chinese medicine. Nat. Med. 17, 1217–1220.
- 14. Hu, K., Guan, W.J., Bi, Y., Zhang, W., Li, L., Zhang, B., Liu, Q., Song, Y., Li, X., Duan, Z., et al. (2020). Efficacy and safety of Lianhuaqingwen capsules, a repurposed Chinese herb, in patients with coronavirus disease 2019: a multicenter, prospective, randomized controlled trial. Phytomedicine 85, 153242.
- Ji, X., Ge, L., Liu, C., Tang, Z., Xiao, Y., Chen, W., Lei, Z., Gao, W., Blake, S., De, D., et al. (2021). Capturing functional two-dimensional nanosheets from sandwich-structure vermiculite for cancer theranostics. Nat. Commun. 12, 1124.
- 16. Bennetzen, J. (2019). Better research for better tea. Nature 566, S5.
- 17. Drew, L. (2019). Making tea. Nature 566, S2–S4.
- 18. Brody, H. (2019). Tea. Nature 566, S1.
- Gilbert, N. (2019). Drink tea and be merry. Nature 566, S8–S9.
- 20. Zhang, X. (2015). Tea and cancer prevention. J. Cancer Res. Updates 4, 65–73.

- Yang, Y., Jin, P., Zhang, X., Ravichandran, N., Ying, H., Yu, C., Ying, H., Xu, Y., Yin, J., Wang, K., et al. (2017). New epigallocatechin gallate (EGCG) nanocomplexes co-assembled with 3mercapto-1-hexanol and β-lactoglobulin for improvement of antitumor activity. J. Biomed. Nanotechnol. 13, 805–814.
- Hara, Y. (2011). Tea catechins and their applications as supplements and pharmaceutics. Pharmacol. Res. 64, 100–104.
- Kim, W., Zhu, W., Hendricks, G.L., Van Tyne, D., Steele, A.D., Keohane, C.E., Fricke, N., Conery, A.L., Shen, S., Pan, W., et al. (2018). A new class of synthetic retinoid antibiotics effective against bacterial persisters. Nature 556, 103–107.
- 24. Tu, Y., Lv, M., Xiu, P., Huynh, T., Zhang, M., Castelli, M., Liu, Z., Huang, Q., Fan, C., Fang, H., et al. (2013). Destructive extraction of phospholipids from *Escherichia coli* membranes by graphene nanosheets. Nat. Nanotechnol. *8*, 594–601.
- Durrant, J.D., Kochanek, S.E., Casalino, L., leong, P.U., Dommer, A.C., and Amaro, R.E (2020). Mesoscale all-atom influenza virus simulations suggest new substrate binding mechanism. ACS Cent. Sci. 6, 189–196.
- Helke, K.L., Nelson, K.N., Sargeant, A.M., Jacob, B., McKeag, S., Haruna, J., Vemireddi, V., Greeley, M., Brocksmith, D., Navratil, N., et al. (2016). Pigs in toxicology: breed differences in metabolism and background findings. Toxicol. Pathol. 44, 575–590.
- Helke, K.L., and Swindle, M.M. (2013). Animal models of toxicology testing: the role of pigs. Expert Opin. Drug Metab. Toxicol. 9, 127–139.
- Li, L., Guo, J., Wang, Y., Xiong, X., Tao, H., Li, J., Jia, Y., Hu, H., and Zhang, J. (2018). A broadspectrum ROS-eliminating material for prevention of inflammation and drug-induced organ toxicity. Adv. Sci. 5, 1800781.